Modular Switched-Capacitor Dc-Dc Converters Tied with Lithium-ion Batteries for Use in Battery Electric Vehicles

Yue Cao, Yutian Lei, *Student Member*, *IEEE*,
Robert C.N. Pilawa-Podgurski, *Member*, *IEEE*, Philip T. Krein[1], *Fellow*, *IEEE*

***Abstract*—This paper presents a modular switched-capacitor (SC) dc-dc converter based electric drive system for battery electric vehicles. In such a system, modularized lithium-ion battery cell tied MOSFET SC converters are used instead of the more conventional IGBT boost converter. Following the drive train architecture, the modeling approach for each electrical component, including the battery set, dc-dc and dc-ac converters, ac machines, and their control is discussed. Emphasis is given on state of the art lithium-ion battery models and SC converter design. System level performance is analyzed based on simulation results across drive cycles. Hardware including a three-cell lithium-ion battery tied SC converter module is built and tested. Application notes such as economic and spacing constraints are addressed.**

***Index Terms*—Switched capacitor dc-dc converters, electric vehicles, lithium-ion batteries, ac motor drives**

I. Introduction

Switched-capacitor (SC) converters are being applied at increasing power levels [l]. Because of the high energy density of capacitors [2], SC converters can enable improved power density compared to conventional inductor-based power converters. This makes SC converters attractive in space-constrained applications such as battery electric vehicles (BEV). Recent technological advances in SC converters [3-8] have greatly reduced their sizes and improved efficiencies while increasing switching frequencies. High power applications utilizing SC converters have also made significant progress [9-11]. However, low-voltage high-current small-sized modular SC converters tied to lithium-ion batteries used in BEV motor drives applications have not been fully explored. In [12], a simulation study on this topic was developed. However, no hardware implementation was made, and the system level efficiency analysis was not thorough in particular regarding the impact of an unregulated dc bus voltage on motor drive's efficiency.

BEV powertrain systems often employ a boost converter to provide a high bus voltage and tight inverter package. Typical battery packs consist of many single-cell lithium-ion batteries, usually 3.2-4.0 V each, depending on their state of charge (SOC) [13]. They are connected in series to form a 300-400 V source, which is boosted to around 700 V for the dc bus [14]. Instead of a single bulky IGBT boost converter between the battery pack and the dc bus, battery-cell-level modular SC converters, based on MOSFETs, were proposed in [12]. These SC converters are connected in series and directly form a 600-800 V dc bus. Since the conversion ratio for a SC converter is fixed by its circuit topology, this strategy yields an unregulated dc bus.

Potential advantages for modular SC converters in the BEV application include reduced volume and weight footprint, improved thermal flows, flexible structures, improved battery cell balancing, increased reliability, and fault bypass modes, etc. However, many other factors are unknown, such as the proposed system's feasibility, efficiency, cost, and also its impact on the motor drive. The contribution of this paper is to design and simulate such a system and analyze its performance. A state-of-the-art SC converter module tied with lithium-ion batteries is designed, built, and tested to validate the concepts. A comparison is made to a conventional boost converter.

II. BEV Drive System with SC Converters

Figure 1 shows the electric drive system considered in this work: the battery supplies a dc bus through a dc-dc converter and then an inverter drives an ac induction machine. In the proposed system, single or multiple battery cells form a module with an SC converter, and the modules connect in series to form a dc bus. This is illustrated in Figures 2 and 3, respectively. Note that there must be multiple columns of modules in parallel so that the current capacity meets the ac drive demand while limiting battery cell discharge currents. A typical rating limit for each battery cell is 1C, i.e., for a 2.2 Ah battery, the rating is 2.2 A.

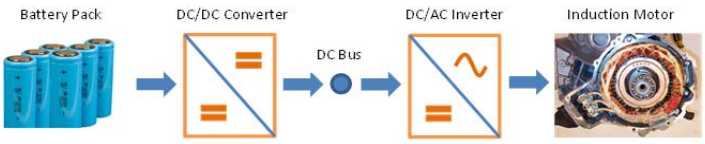

Figure 1. Existing battery electric vehicle power system structure.

Figure 2. A single battery cell and an SC converter formed power module.

[1]Yue Cao, Yutian Lei, Robert C.N. Pilawa-Podgurski, and Philip T. Krein are with the Department of Electrical and Computer Engineering, Universityof Illinois, Urbana, IL 61801, USA (email: yuecao2@illinois.edu, lei10@illinois.edu, pilawa@illinois.edu, krein@illinois.edu).

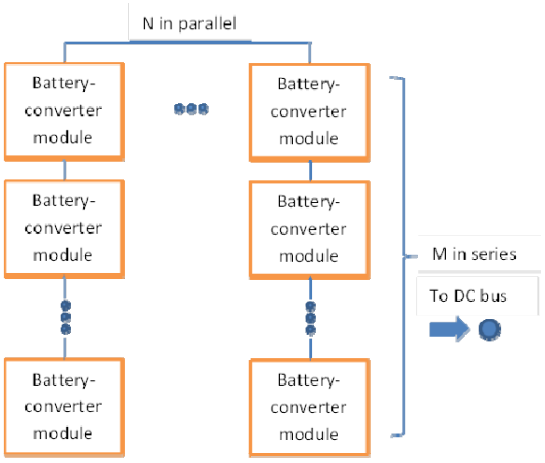

Figure 3. Series and parallel structure for proposed battery-converter modules.

A 1:2 boost SC converter is chosen for the study. A 1:3 (or 2:5 or 1:N) boost SC converter may be also used to reduce the number of series-connected battery cells. However, SC converters with conversion ratios above 1:3 may be challenging to implement in practice. This is because, although the number of series battery cells is reduced, the number of parallel battery cells is increased to match the total power output. The number of SC converters remains the same as a result, but the number of semiconductor devices increases in each converter as the conversion ratio increases, which increases the converter cost and potentially reduces the reliability.

The 1:2 SC converter topology is shown in Figure 4. It uses four switches controlled by complementary gate signals (*Q1* and *Q2*), which have a duty ratio of 50% and negligible dead time. In Phase 1, *Q2* and *Q4* are on, connecting V_{in} and *Cc* in parallel. Thus the flying capacitor *Cc* is charged to V_{in}. In Phase 2, *Q2* and *Q4* are off, and *Q1* and *Q3* are on. V_{in} and *Cc* are connected in series, resulting an output voltage of twice V_{in}. The flying capacitor provides the intermediate voltage so that *Q1* to *Q4* only need to be rated at V_{in} (as opposed to V_{out} for a conventional boost converter).

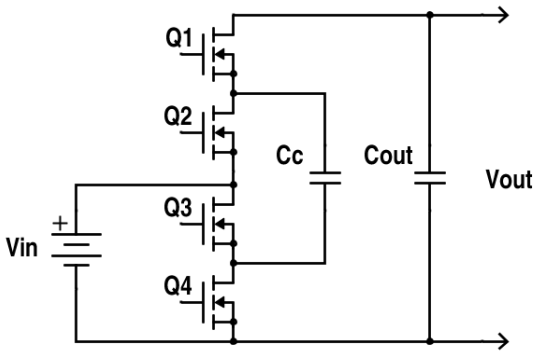

Figure 4. A 1:2 boost SC converter circuit topology.

The battery model is based on the circuit in Figure 5 [15]. The second, minute, and hour based resistors and capacitors predict battery cell dynamics in each of the corresponding time frames. The transfer function of the battery terminal voltage is then given as

$$V_t = V_{oc} - I_c\left(R_{series} + R_{ts} \| \frac{1}{sC_{ts}} + R_{tm} \| \frac{1}{sC_{tm}} + R_{th} \| \frac{1}{sC_{th}}\right) \quad (1)$$

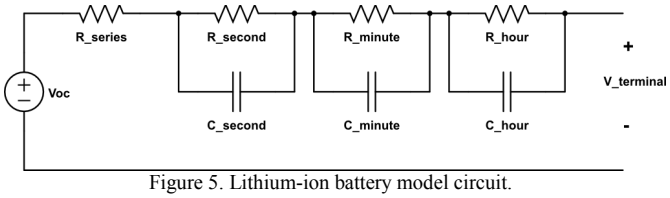

Figure 5. Lithium-ion battery model circuit.

The voltage source, resistors, and capacitors depend nonlinearly on the battery state of charge (SOC). In [15], *V*, *C*, and *R* values are modeled as sixth-order polynomials of SOC. An improved set of *V*, *C*, and *R* values adopted from [16] are used in this paper, which address the fitted polynomial instability issues. To remedy this, a logarithmic interpolation equation

$$\ln(V, C, R) = a_0 + a_1 \ln(SOC) + \ldots + a_6 \ln^6(SOC) = \sum_{k=0}^{6} a_k \ln^k(SOC) \quad (2)$$

is employed. The new method produces more accurate *V*, *C*, *R* values and models the battery more robustly. The coefficients of (2) are listed in Table I. The labels (C) and (D) indicate coefficients for charging and discharging conditions. These values are from the single-cell data that were extracted from measurements of Panasonic CGR18650A 3.7 V, 2.2 Ah Li-ion batteries [16-17].

The SOC is modeled based on

$$SOC(t) = SOC_{initial} + \int_0^t f_1[i_{charge}(t)] \times i_{charge}(t)dt + \int_0^t f_2[i_{discharge}(t)] \times i_{discharge}(t)dt \quad (3)$$

where the initial SOC is constant and defined prior to simulation, *i(t)* is the instantaneous discharging or charging current, and *f* is a function of that current and modeled as a lookup table. The relationships between *f* and *i* are given in Tables II and III for the charging and discharging [16].

Table I. Coefficients for functions used in Figure 5 and Equation (2).

	a0	a1	a2	a3	a4	a5	a6
Voc	1.4222	0.2214	0.1829	0.0745	0.0145	0.0014	5×10^{-5}
Rseries (D)	-2.9384	-0.2328	-0.2109	-0.1294	-0.0302	0	0
R_s (D)	-3.4883	-1.2434	-0.5619	0.0044	0.0348	0	0
C_s (D)	-0.146	0.3731	1.6511	1.0513	0.1918	0	0
R_m (D)	-3.1892	-0.0486	1.4851	6.1491	7.0124	3.1645	0.4997
C_m (D)	6.9413	-6.5951	-29.577	-56.356	-46.582	-16.991	-2.2588
Rseries (C)	-2.8108	0.6011	0.8951	0.436	0.07	0	0
R_s (C)	-3.5637	0.0016	3.4633	4.6412	2.2718	0.425	0.0188
C_s (C)	-0.2737	-3.4945	-14.705	-21.767	-14.113	-4.1803	-0.4632
R_m (C)	-2.8744	1.1014	1.1243	0.266	-0.1345	-0.046	0
C_m (C)	6.9622	-0.447	2.896	4.5575	2.2427	0.3544	0
R_h	-5.6352	5.1517	12.006	6.1973	0	0	0
C_h	14.622	-6.2451	-19.818	-11.446	0	0	0

Table II. *f* and *i* relationship for the charging state in Equation (3).

i (charge)	0	0.0838	0.4386	1.0988	2.202
f(i)	1.34×10^{-4}	1.3259×10^{-4}	1.2581×10^{-4}	1.2391×10^{-4}	1.2192×10^{-4}

Table III. *f* and *i* relationship for the discharging state in Equation (3).

i (discharge)	0	0.0808	0.4389	1.0886	2.1603
f(*i*)	-1.4×10^{-4}	-1.3751×10^{-4}	-1.2727×10^{-4}	-1.3222×10^{-4}	-1.3928×10^{-4}

The induction machine (IM) is modeled in the classical d-q reference frame [18]. A field oriented controller (Figure 6) is implemented in the IM drive (Figure 7).

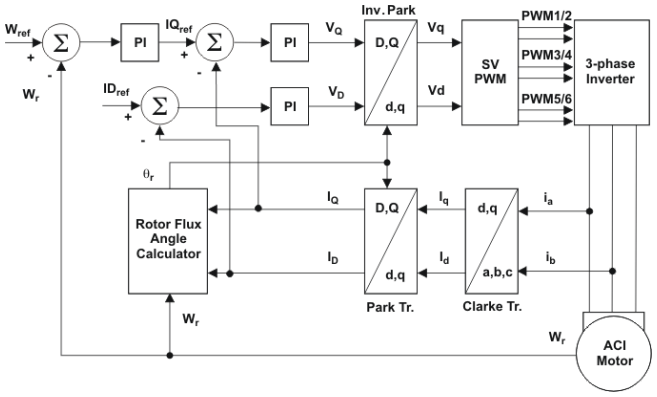

Figure 6. Induction machine field oriented control diagram.

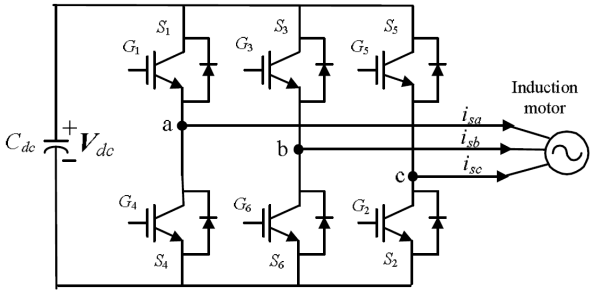

Figure 7. Dc-ac inverter circuit tied to the ac motor.

III. Simulation Setup

A comprehensive simulation must be run for the integrated system. It is important to evaluate performance under real-life scenarios, which include the variations in battery SOC, output powers, etc. Each of the system components mentioned in Section II needs to be designed with realistic requirements. The objective is to power a 460 V ac induction machine up to about 100 kW (134 HP) for automotive applications. For this simulation study, without loss of generality, a converter rated up to 10 kW (1/10 scale) will be developed. Higher power requires more parallel battery branches and would slow the simulation without adding insight. The power flowing through each SC converter module is unchanged compared to a full-scale system.

One focus for this paper is the design of the SC converter. A conventional SC converter design is chosen since advanced topologies and techniques usually incur additional cost. The efficiency of an SC converter is determined by the output impedance of the converter. The output impedance at low switching frequencies (slow switching limit, SSL) is

$$R_{SSL} = \sum_{capacitors} \frac{(a_{c,i})^2}{C_i f_{sw}} \tag{4}$$

The output impedance at high switching frequencies (fast switching limit, FSL) is

$$R_{FSL} = 2 \sum_{switches} R_i (a_{r,i})^2 \tag{5}$$

where $a_{c,i}$ is the charge multiplier through each flying capacitor C_i, and $a_{r,i}$ is the charge multiplier through each switch with resistance R_i [19]. An optimal design trades off the R_{ds} of the switches, the flying capacitor C_c and the switching frequency such that R_{SSL} is similar to R_{FSL}, and also such that the conduction loss and switching loss are comparable.

For this particular application, 15 V 12 A MOSFETs are used, which have R_{ds} of 9.4 mΩ each. A nominal switching frequency of 500 kHz is selected. Hence C_c is calculated to be about 80 µF. The expression for the output capacitor is determined by the output voltage ripple [19], such that

$$C_{out} = \frac{0.5 I_{out}}{f_{sw} \Delta V_{out}} \tag{6}$$

The targets here are 1.1 A (0.5C) of continuous output current and a voltage ripple of 0.05 V for each SC converter module. Hence C_{out} is found to be 110 µF.

The 460 V ac induction machine requires a minimum 650 V dc bus. In order to achieve this voltage, approximately 90 Panasonic lithium-ion batteries need to be connected in series. In the proposed system, 30 SC converter modules, each designed for 12 V to 24 V conversion (3 series cells at each input) are used. At least 5 parallel branches need to be formed to produce nominal power of 4.3 kW at 1C current. A current of 2.3C will be needed when 10 kW is required. For the comparison study of a conventional dc-dc boost converter, 1200 V 50 A IGBTs and 10 kHz switching frequency are used. The dc-ac inverter and the ac induction machine are held the same for both SC converter and conventional boost converter topologies.

IV. Simulation Results and Analysis

To demonstrate the capabilities of the integrated system, a transient followed by a steady state response is simulated in the MATLAB/Simulink environment. Figure 8 shows the acceleration of the induction machine from 0 to about 187 rad/sec (1780 RPM). The figure also shows the stator current (the inverter output current). A steady-state torque of about 20 Nm indicates the output power is approximately 3750 W, demonstrating nominal operation at approximately 1C (2.2 A). Figure 9 shows the input and output voltage waveforms of the battery-SC converter module as well as the battery output current of a three-cell fully charged (1.0 SOC) battery pack. These waveforms track closely as expected. Looking more closely, it can be observed that the output voltage ripple is about 0.05 V, consistent with the design target. Figure 10 shows the input and output voltages of the inverter and the modulation index required to operate the induction machine. The dc bus voltage is well below 760 V initially because of the high initial acceleration current pulling down the battery terminal voltage.

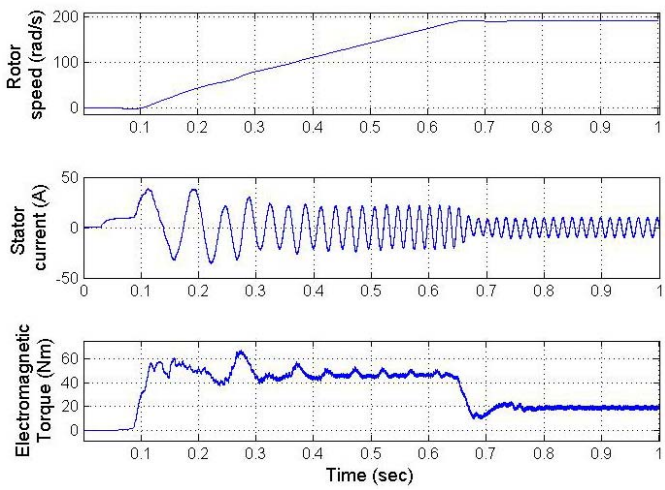

Figure 8. Induction machine speed, current, and torque during acceleration.

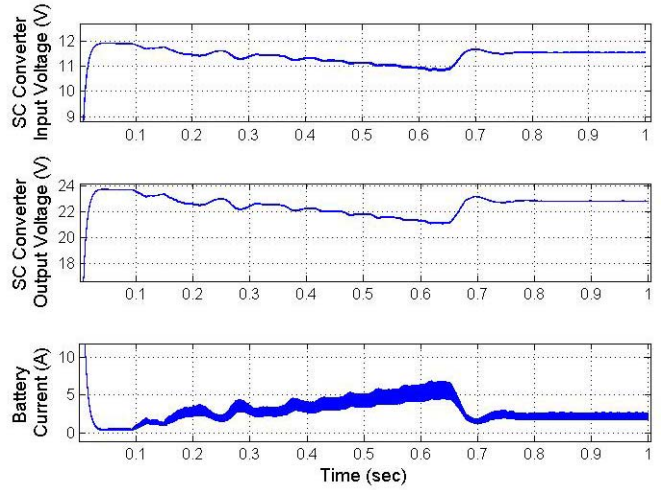

Figure 9. SC converter input/output voltages and battery current.

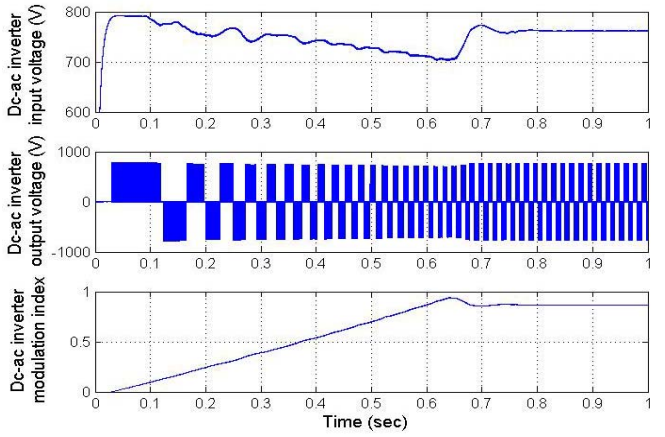

Figure 10. Dc-ac inverter input/output voltage and its modulation index.

Table IV presents selected dc-dc conversion efficiencies when battery SOC and output current change, based on the simulation results. From the table, battery SOC has little impact on converter efficiency, and SOC = 1 will be used for remaining comparisons. Figure 11 shows the efficiencies from the two dc-dc converters versus battery output currents when the SOC is 1.0. The results show that the SC converter outperforms the boost converter under light loads, but drops above about 1.6C give the heavy-load advantage to the conventional converter. In a typical transportation drive cycle, time at high power is limited, so long-term operation will favor the SC converter.

Table IV. SC converter (left number) and boost converter (right number) efficiency at different battery SOCs and currents.

	1.0 A out	2.0 A out	3.0 A out	4.0 A out	5.0 A out
1.0 SOC	93.2/81.6%	96.3/89.5%	93.6/90.4%	89.8/92.1%	87.2/92.7%
0.9 SOC	93.3/80.7%	96.3/88.9%	93.6/90.5%	89.8/91.9%	87.2/92.5%
0.8 SOC	93.3/80.9%	96.4/88.4%	93.7/90.5%	89.9/91.9%	87.3/91.6%
0.7 SOC	93.3/81.8%	96.4/87.3%	93.7/90.7%	89.9/91.9%	87.3/91.6%
0.6 SOC	93.4/79.0%	96.4/87.2%	93.7/90.5%	89.9/90.8%	87.3/91.6%
0.5 SOC	93.3/78.4%	96.3/87.5%	93.6/90.6%	89.8/90.9%	87.2/91.6%

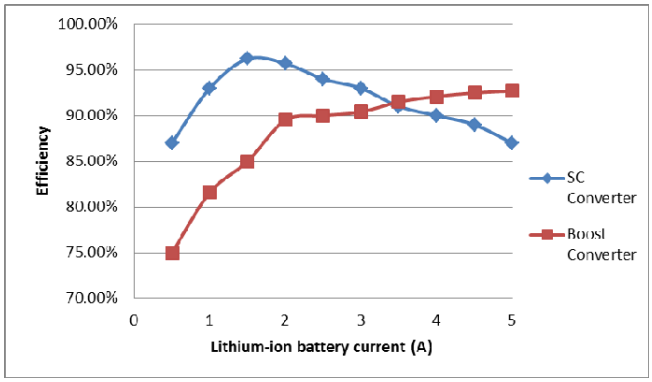

Figure 11. SC and boost converters efficiencies versus battery output currents.

Although the ac motor drive is not the focus of this paper, its performance is impacted in the SC converter system because of the variable dc bus voltage. This is not the concern for the boost converter system since it can regulate its output. Figure 12 shows the ac motor drive efficiency, computed as mechanical output power divided by inverter input power, versus battery cell SOC in the SC converter power train system. This sample lithium-ion battery technology varies from about 3.5 V to about 4.0 V per cell while the SOC is from 0.1 to 1.0, and the dc bus varies only about 12%. The efficiency curve in Figure 12 varies within only about 3%. The difference comes from the change of modulation indices on the inverter and from power factor changes in the machine.

The overall system efficiency, defined as the output mechanical power divided by the output battery power, can be found by combining the dc-dc converter and ac motor drive efficiencies. Efficiency maps with battery cell SOC and current as independent variables are drawn for the SC converter system and the boost converter system in Figure 13 and Figure 14, respectively. Both systems have preferred operation regions, but the SC converter system is more efficient over a wider range. This is supported by the efficiency difference plot (SC minus boost) in Figure 15. Depending on drive cycles encountered by the vehicle, energy savings will be several percent with the SC system.

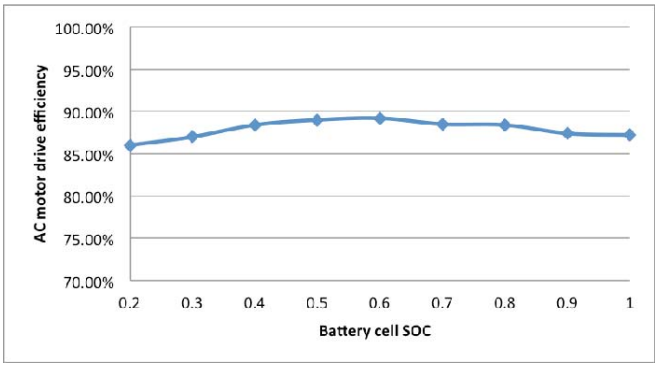

Figure 12. Ac motor drive efficiencies versus battery cell SOC in the SC converter power train system.

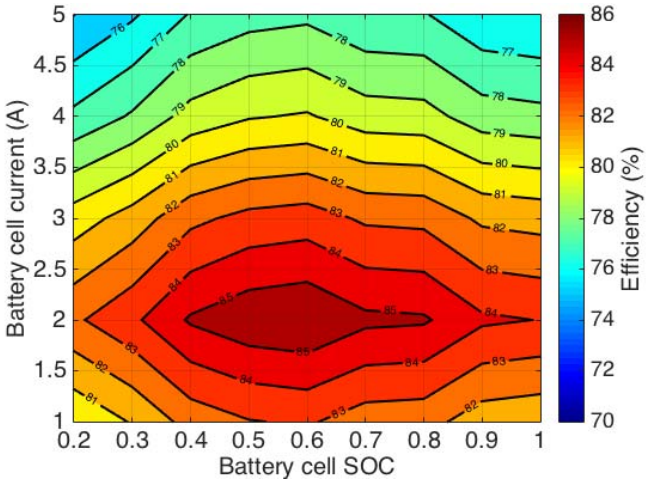

Figure 13. System efficiency map for the SC converter power train.

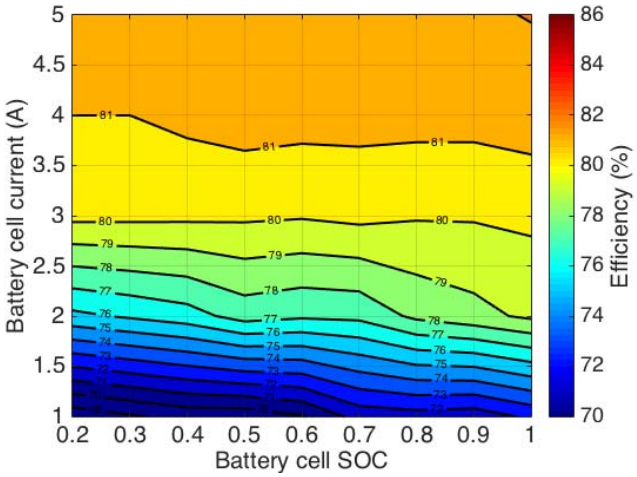

Figure 14. System efficiency map for the boost converter power train.

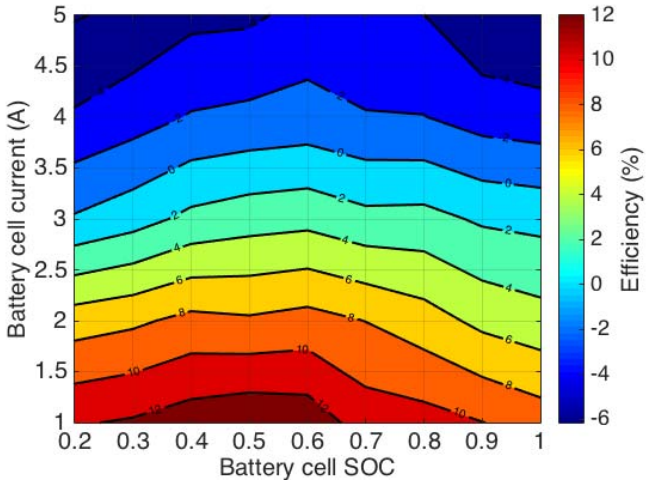

Figure 15. Efficiency difference map between two converter systems (SC converter minus boost converter).

V. SC Converter Module Hardware Implementation

A state of the art 12 V to 24 V SC converter utilizing fast switching DrMOS (driver integrated MOSFET) has been built [4]. A DrMOS module consists of a pair of half-bridge connected MOSFETs as well as the necessary gate drive circuitry in one IC package. A 1:2 SC converter needs two DrMOS modules and can have significantly reduced components count compared to a discrete solution. A complete component listing is given in Table V.

Table V. Hardware cost comparison between SC and boost converters.

Component	Part number	Value
MOSFET	2 of CSD95379Q3M	20V 20A half-bridge plus driver
Flying capacitor, Cc	2 of C3216X5R1E476M160AC	47uF 25V X5R
Input capacitor, Cin	C3216X5R1E476M160AC	47uF 25V X5R
Output capacitor, Cout	2 of C3216X5R1E476M160AC	47uF 25V X5R
Level-shifter	ADUM5210	-
Microcontroller	Piccolo 280F035	-

One module of three-cell lithium-ion battery and SC converter is shown in Figure 16. Figure 19 illustrates a screenshot of the input/output voltage and current under the nominal condition (2.2 A). The module's efficiency, defined as the output power to the dc bus divided by the power from the lithium-ion batteries, is tested against a variety of loads and is plotted in Figure 20. Note that the measured efficiency curve is close to the simulation result in terms of shape and value. Thermal images of the module under the nominal load (2.2 A) and highest load (4.8 A) are shown in Figure 17 and Figure 18, respectively. The temperature range indicates that no extra cooling unit is required and that natural convective cooling is sufficient.

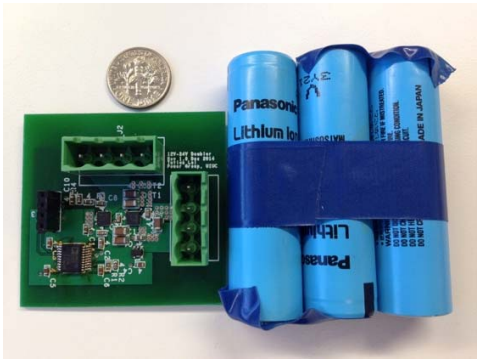

Figure 16. Battery-SC converter module.

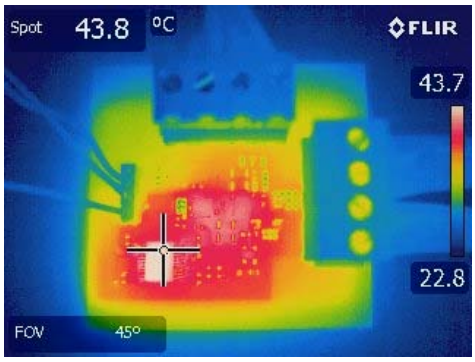

Figure 17. SC converter thermal image under nominal load.

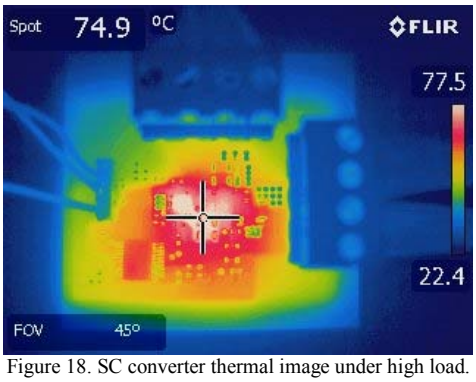

Figure 18. SC converter thermal image under high load.

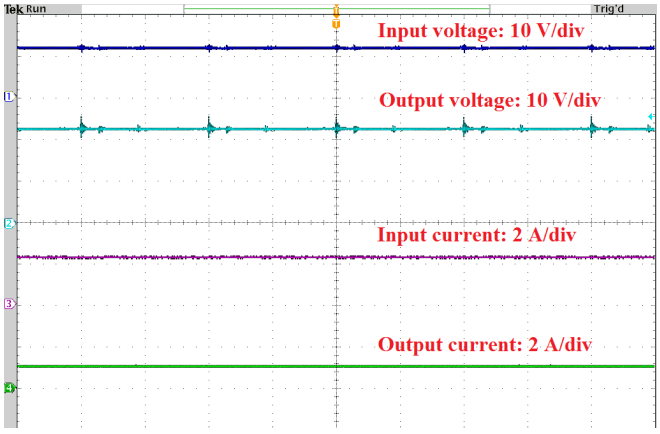

Figure 19. Input and output voltage/current oscilloscope waveforms.

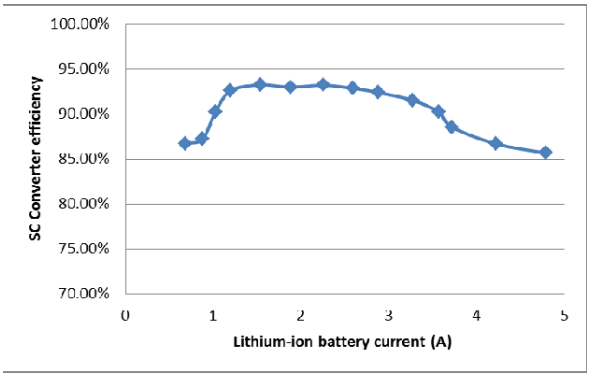

Figure 20. Measured SC converter efficiency under different loads.

One major concern is cost. The cost for all the SC converters in a vehicle system is expected to be more than that of a single boost converter based on system complexity and parts count. This cost estimate depends on the power requirement of the vehicle. Since the SC converters are not likely to need heat sinks and can be integrated with batteries as modular units, overall costs may be improved with an SC system. A more complete cost study requires a defined drive cycle and comprehensive implementation and is beyond the scope of this paper. The modularity provides more flexibility and system reliability in case of faults.

VI. Conclusion

A battery electric vehicle traction system utilizing lithium-ion batteries, switched capacitor converters, an inverter and an ac induction machine has been modeled and simulated under various operating conditions, including transient and steady-state analysis. A similar system with a conventional boost converter is also simulated for comparison purposes. The results show that the SC converter topology based system yields higher efficiencies under nominal or light loads, whereas the boost converter topology based system is more efficient at heavy loads. A hardware test module was built for efficiency verification and spacing, thermal, and economics analysis. The SC converter reduces hardware space required and no additional cooling equipment is necessary, leaving more room for extra energy storage. From the economic perspective, the SC converter costs more, but this may be traded off in the long run. The trade off study will vary depending on user needs. Future work on this topic includes regenerative braking and battery charging and their simulation at the system level. In addition, the SC converter can be integrated with a battery management system for cell balancing.

VII. Acknowledgement

This work was supported by the Grainger Center for Electric Machinery and Electromechanics at the University of Illinois and by the Power Affiliates Program (PAP) at Illinois.

REFERENCES

[1] A. Ioinovici, "Switched-capacitor power electronics circuits," *IEEE Circuits and Systems Magazine*, vol. 1, issue 3, pp. 37-42, 2001.

[2] C. Barth, I. Moon, Y. Lei, S. Qin, R.C.N. Pilawa-Podgurski, "Selection of capacitors for power buffering in single-phase inverter applications," in *Proc. IEEE Energy Conversion Congress and Expo*, 2015.

[3] J. W. Kimball and P. T. Krein, "Analysis and design of switched capacitor converters," in *Proc. IEEE Applied Power Electronics Conf.*, 2005, pp. 1473-1477.

[4] Y. Lei and R.C.N. Pilawa-Podgurski, "Soft-charging operation of switched-capacitor DC-DC converters with an inductive load," in *Proc. IEEE Applied Power Electronics Conf.*, 2014, pp. 2112-2119.

[5] B.B. Macy, Y. Lei, and R.C.N. Pilawa-Podgurski, "A 1.2 MHz, 25 V to 100 V GaN-based resonant Dickson switched-capacitor converter with 1011 W/in3 (61.7 kW/L) power density," in *Proc. IEEE Applied Power Electronics Conf.*, 2015, pp. 1472-1478.

[6] Y. Lei and R.C.N. Pilawa-Podgurski, "A General Method for Analyzing Resonant and Soft-Charging Operation of Switched-Capacitor Converters," *IEEE Trans. Power Electronics*, vol. 30, issue 10, pp. 5650-5664, 2015.

[7] R.C.N. Pilawa-Podgurski and D.J. Perreault, "Merged Two-Stage Power Converter With Soft Charging Switched-Capacitor Stage in 180 nm CMOS," *IEEE Journal of Solid-State Circuits*, vol. 47, issue 7, pp. 1557-1567, 2012.

[8] C. Schaef, K. Kesarwani, and J.T. Stauth, "20.2 A variable-conversion-ratio 3-phase resonant switched capacitor converter with 85% efficiency at 0.91W/mm2 using 1.1nH PCB-trace inductors," in *Proc. IEEE Solid-State Circuits Conf.*, 2015.

[9] F. Z. Peng, F. Zhang, and Z. Qian, "A magnetic-less DC-DC converter for dual-voltage automotive systems," *IEEE Trans. Industry Applications*, vol. 39, pp. 511-518, March-April 2003.

[10] M. Shen, F. Z. Peng, and L. M. Tolbert, "Multilevel DC–DC power conversion system with multiple DC sources," *IEEE Trans. Power Electronics*, vol. 23, pp. 420-426, January 2008.

[11] L. Fu, X. Zhang, F. Guo, and J. Wang, "A phase shift controlled current-fed Quasi-Switched-Capacitor isolated dc/dc converter with GaN HEMTs for photovoltaic applications," in *Proc. IEEE Applied Power Electronics Conf.*, 2015, pp. 191-198.

[12] Y. Cao and Z. Ye, "Simulation and analysis of switched capacitor dc-dc converters for use in battery electric vehicles," in *Proc. IEEE Power and Energy Conf. at Illinois*, 2015.

[13] X. Chen, et al., "An overview of lithium-ion batteries for electric vehicles," in *Proc. IEEE Power and Energy Conf.*, 2012, pp. 230-235.

[14] B. Bural, et al., "An experimental comparison of different topologies for fuel-cell, battery and ultra-capacitor in electric vehicle," in *Proc. IEEE National Conf. on Electrical, Electronics, and Computer Engineering*, 2010, pp. 46-52.

[15] R. C. Kroeze and P. T. Krein, "Electrical battery model for use in dynamic electric vehicle simulations," in *Proc. IEEE Power Electronics Specialists Conf.*, 2008, pp. 1336-1342.

[16] Y. Cao and P. T. Krein, "An average modeling approach for mobile refrigeration hybrid power systems with improved battery simulation," in *Proc. IEEE Transportation Electrification Conf.*, 2013.

[17] [Online]. Available: http://articles.sae.org/12833/

[18] P. C. Krause, O. Wasynczuk, and S. D. Sudhoff, *Analysis of Electric Machinery and Drive Systems*, 2nd ed. Edison, NJ: Wiley-IEEE Press, 2002, pp. 525-556.

[19] M. Seeman and S. R. Sanders, "Analysis and optimization of switched-capacitor dc-dc converters," *IEEE Trans. Power Electronics*, vol. 23, no. 2, pp. 841-851, March 2008.